RESEARCH ARTICLE | OCTOBER 19 2023

The effect of melt flow rate and print speed on the density and microcellular structure of 3D printed polylactic acid foams FREE

Karun Kalia; Alireza Amirkhizi; Amir Ameli

AIP Conf. Proc. 2884, 140003 (2023)
https://doi.org/10.1063/5.0168370

The Effect of Melt Flow Rate and Print Speed on the Density and Microcellular Structure of 3D Printed Polylactic Acid Foams

Karun Kalia[1 a)], Alireza Amirkhizi[2 b)], Amir Ameli[1 c)]

[1] *Department of Plastics Engineering, University of Massachusetts Lowell, 1 University Ave, Lowell, MA 01854, United States of America*
[2] *Department of Mechanical Engineering, University of Massachusetts Lowell, 1 University Ave, Lowell, MA 01854, United States of America*

[a)] *Karun_Kalia@student.uml.edu*
[b)] *Alireza_Amirkhizi@uml.edu*
[c)] *Corresponding author: Amir_Ameli@uml.edu*

Abstract. The purpose of this study was to investigate the effect of flow rate and print speed on the density and microcellular structure of polylactic acid (PLA) foams printed via fused filament fabrication (FFF) process. Unexpanded filaments loaded with thermally expandable microspheres (TEMs), at 2.5 wt.%, were prepared as a feedstock for in-situ foam printing process. Foam samples were printed at three different nozzle-exit flow rate levels (i.e., 55, 85 and 100%) and at three print speed levels (i.e., 5, 25 and 125 $mm.s^{-1}$) and their density, surface, and internal cellular microstructure were studied. It was found that both process factors have significant effects on the part density, cellular morphology, and mesostructure. With a decrease in the flow rate from 100 to 55%, the part density proportionally decreased from 0.79 to 0.56 $g.cm^{-3}$. Whereas the part density was relatively high (0.95 $g.cm^{-3}$) at the high print speed of 125 $mm.s^{-1}$, low densities (0.67-0.71 $g.cm^{-3}$) were obtainable at low print speed range of 5-25 $mm.s^{-1}$. Moreover, the highest cell density was obtained at the medium level of both flow rate and print speed. The correlation between the process factors (flow rate and print speed) and properties (density and cellular microstructure) were explained in terms of the melt residence time inside the heater block as well as the melt volumetric throughput. Overall, at the medium levels of flow rate and print speed, the printed foams provided the lowest density and highest uniformity in the morphology.

Keywords: foam, 3D printing, fused filament fabrication, thermally expandable microsphere, flow rate, print speed

Introduction

Polymer foams have numerous applications for lightweighting, insulation, energy absorption and damping, etc. in various industries [1]. Thermoplastic-based foam products are usually made using physical [2] and chemical [3] blowing agents, and more recently, thermally expandable microspheres (TEMs) [4][5]. Polymer foaming has been successfully integrated in injection molding [6][7] and extrusion [8][9] processes with mature technologies and numerous applications. However, with the traditional manufacturing techniques, it is not easy to manufacture complex, customized, and/or functionally graded foam parts, as it would require significant modifications and financial investment to meet such requirement.

Material extrusion (MEX) additive manufacturing (AM) also known as fused filament fabrication (FFF)is the most common AM technology used in the fabrication of polymers. FFF basically integrates two classical fabrication techniques of extrusion and fusion or welding in a layered fashion, facilitating the realization of complex geometries with more flexibility in design and customization[10]. Coupling polymer foaming and MEX AM can result in an innovative framework to produce foamed products from various thermoplastics [11][12].

Several approaches have been used to obtain cellular structures in an FFF part, most of which are not truly through in-situ foaming process [13][14][15][16]. In-situ foam printing is referred to a method where first a foaming

Proceedings of the 37th International Conference of the Polymer Processing Society (PPS-37)
AIP Conf. Proc. 2884, 140003-1–140003-9; https://doi.org/10.1063/5.0168370
Published by AIP Publishing. 978-0-7354-4705-9/$30.00

agent is introduced to the polymer matrix during the filament fabrication and then the blowing agent is activated during the printing process to incur foaming. This method basically enables simultaneous foaming and printing [17][18]. In our recent work, we have established a method of expandable filament fabrication for polylactic acid (PLA) and demonstrated the feasibility of in-situ foam 3D printing of such filaments with highly uniform cellular morphology [18]. The literature suggests significant effects of FFF print process parameters on the physical properties of solid unfoamed 3D printed parts [19][20]. However, such in depth investigations about this process is still lacking as foam 3D printing technology is still emerging. It will be key to understand the influence of the printing process parameters on the properties of the resultant foams in order to better design and optimize the process.

To move foam 3D printing process to next steps, the thorough study of the process-structure-properties relationships must be conducted. The focus of this study is to characterize and understand the effect of nozzle-exit flow rate and print speed on the bulk density and cellular structure of the printed foams. Unexpanded PLA filament, at a TEM loading of 2.5 wt.% was made with a regular extrusion process. A flow rate range of 55-100% and a print speed range of 5-125 $mm.s^{-1}$ were used to print various foam parts in order to study their effects on the density, surface features, and internal cellular morphology. Cellular morphologies were characterized with cell size and cell density using cross-sectional scanning electron microscopy (SEM) images of filament and printed foamed samples. The correlation between the process factors (flow rate and print speed) and properties (density and cellular microstructure) were further discussed and optimum values of the process factors were identified.

Experimental Procedure

Materials: NatureWorks PLA grade, Ingeo 4043D was used as the base polymer matrix. PLA 4043D, an extrusion grade, has an MFR of 6 $g.(10min)^{-1}$ and relative viscosity of 4.0. The melting point, glass transition temperature, and density of the utilized PLA are 145-160 °C, of 55-60 °C, and 1.24 $g.cm^{-3}$. (Advancell P501E1 provided by Sekisui was used as the foaming agent. It is a 50 wt.% masterbatch of TEM with polyethylene(PE). According to the manufacturer, the particle size of the microspheres ranges from 21 to 31 μm and the bulk density is 1.10 $g.cm^{-3}$. The microspheres have a core-shell structure. The shell is made of acrylonitrile co-polymer and the core contains liquid hydrocarbon. The TEM's expansion starting temperature range is 160-180 °C and its maximum temperature range is 210-230 °C. The density can be as low as 0.01-0.03 $g.cm^{-3}$ after full expansion of the TEMs. Triethyl citrate (TEC), W308307 with a molecular weight of 276 $g.mol^{-1}$ was purchased from Sigma Aldrich and used as the plasticizer.

Fabrication of unexpanded filaments: Figure 1 shows the filament fabrication process. PLA was dry blended with the TEM masterbatch (2.5 wt.% TEM and 2.5 wt.% PE carrier). Also, TEC was added at 2.0 wt.% as the plasticizer. The formulation is denoted as PLA/TEC/TEM2.5%. E30P Dr. Collin extruder was used to make the filaments. The extruder had a screw with 30 mm of diameter of 750 mm of length. The program included an Igel/Maddock profile to increase the mixing [21]. An additional thermocouple was also used to measure the temperature right before the die exit, denoted as T_{Die}. Extruded filaments were passed through an ice/water bath and collected using a Filabot spooler with a diameter of 1.5±0.05 mm. The barrel temperature for zones 1 to 5 was 145, 155, 152, 138, and 127 °C, respectively. The measured melt temperature and melt pressure at the die was 161±2 °C and 205±5 bar, respectively. More details about the unexpanded filament fabrication process can be found in [18].

Foam fused filament fabrication process: Fabricated PLA/TEC/TEM2.5% filament was used for 3D printing process. Figure 2 (a) schematically illustrates the foam 3D printing process in X-Z plane. TEM particles inside the polymer melt expand while getting extruded from the heater block assembly. Figure 2 (b) shows an example of a foamed dog bone sample with a scanning electron microscopy image revealing the internal cellular structure. ASTM D638 standard Type V specimen was selected, designed in SolidWorks and sliced using Ideamaker slicing software. A Raise 3D Pro 2 3D printer was used with no modification. In this study, flow rate and print speed were variable process parameters. While the print speed was varied, flow rate was kept constant at the middle value, i.e., 85%. Similarly, while the flow rate was varied, print speed was kept constant at its middle value of 25 $mm.s^{-1}$. Table 1 gives the variable process factors used during the 3D printing of the foams. The values for the fixed parameters were 0.8 mm, 0.8 mm, 55 °C, 200 °C, and 0.3 mm for nozzle diameter, raster width, bed temperature, nozzle temperature, and layer height, respectively.

Figure 1. Single-screw extrusion setup with cooling bath and filament spooler used for the fabrication of unexpanded filaments.

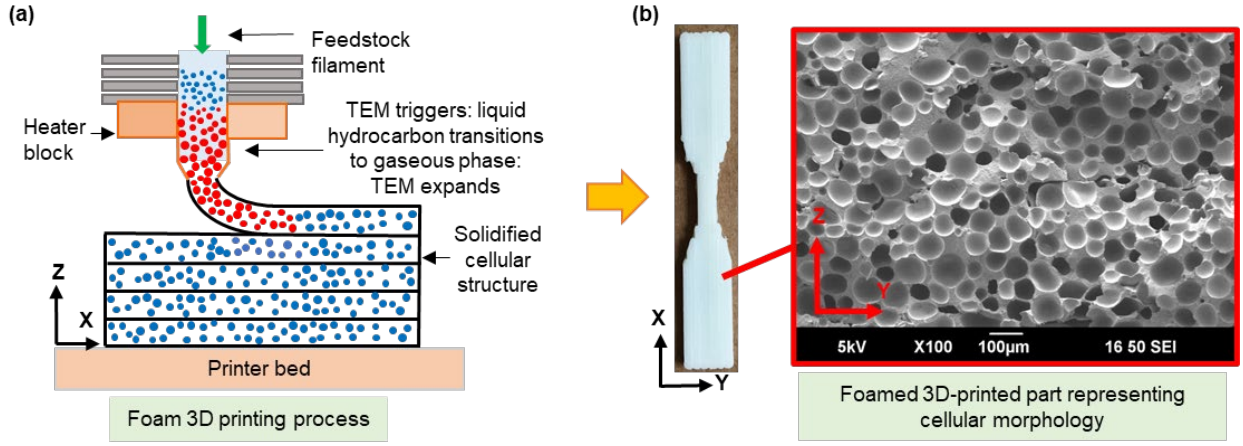

Figure 2. (a) Schematic of foam 3D printing process and (b) a printed dog-bone tensile sample in Y-X plane with a cross-sectional SEM image taken in Y-Z plane representing a foamed microcellular structure.

Table 1. Foam 3D printing process parameters

Parameter	Values
Flow rate (%)	55, 85, 100
Print speed (mm.s^{-1})	5, 25, 125

Characterizations: To reveal the surface appearance of the foams, a Dino-Lite AM2111-0.3MP USB digital microscope was used. SEM was also used for analyzing the internal cellular microstructure of the printed foams. The SEM samples were first sputter coated with gold using a Denton vacuum sputter coater, and a JEOL JSM 6390 SEM was then used for the imaging. Cell size and cell density were obtained by the image analysis of the SEM micrographs. Density was measured using a Mettler Toledo MS303TS kit following the ASTM D792 standard. Three samples were examined for each condition and the means are reported with their standard deviations.

Results and Discussion

The effect of flow rate: Figure 3 and Figure 4 show the surface and the internal microstructure, respectively, of the foam samples printed at three different flow rates. In the parts printed at 55% flow rate, the surface exhibited clear inter-bead line gaps along the print direction (Figure 3a). Similarly, inter-bead gaps and boundaries were also formed in the internal structure, as identified in Figure 4a. When the melt flow rate was raised from 55 to 85%, the inter-bead gaps faded away in both the surface (Figure 3b) and the internal microstructure (Figure 4b) of the prints. Both the surface and the cellular morphology appeared to be more uniform when the part was printed at 85% flow rate. Further increase of the flow rate to 100% resulted in the appearance of some parallel linear marks on the surface (Figure 3c) and decreased the uniformity of the cell morphology (Figure 4c). These linear marks were the consequent of over-extrusion.

Figure 5a shows the calculated cell size and cell density obtained by the image analysis of the SEM micrographs for the foam samples printed at three different flow rates. Parts printed at 55% flow rate showed the highest cell size (56.87 μm) but the lowest cell density (1.25×10^6 cells.cm^{-3}). Once the flow rate was changed from 55 to 85%, the cell size was lowered to 50.54 μm and the cell density was increased to 3.15×10^6 cells.cm^{-3}. Further increase of the flow rate to 100% resulted in opposite trends, i.e., the cell size slightly increased to 52.48 μm and the cell density decreased to 2.04×10^6 cells.cm^{-3}. Moreover, Figure 5b gives the printed foam overall density as a function of the flow rate. With an increase in the flow rate from 55% to 100%, the part density continuously increased from 0.56 to 0.79 g.cm^{-3}. The part density reflects the overall weight reduction due to the foaming as well as the inter-bead voids if they are present.

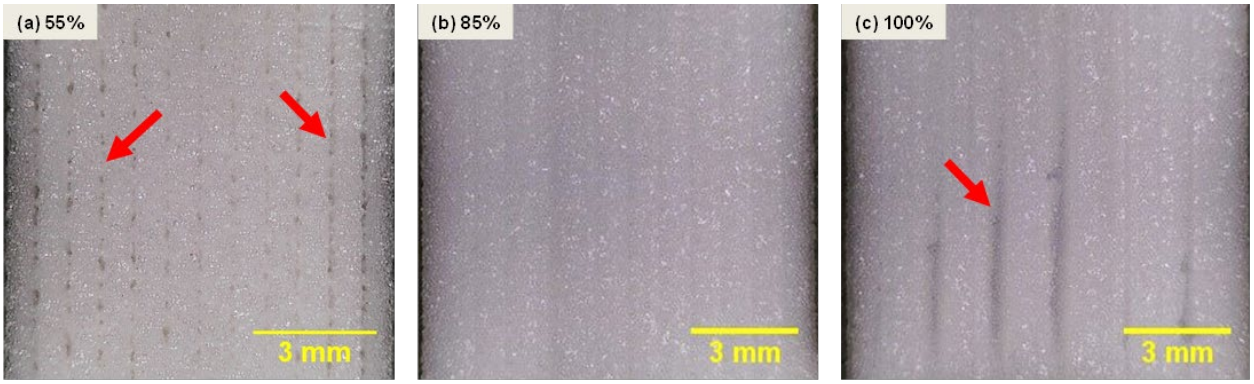

Figure 3. Optical images (Y-X plane view) showing the surface morphology of foam samples printed at (a) 55, (b) 85, and (c) 100% flow rate.

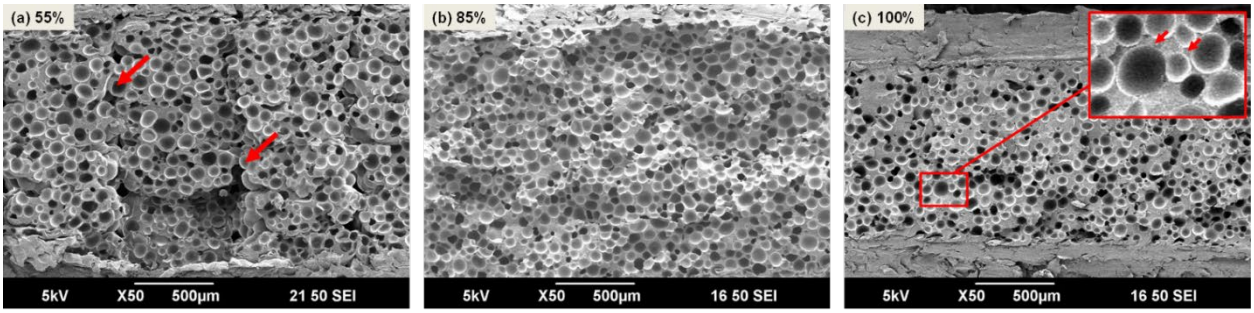

Figure 4. SEM micrographs (Y-Z plane view) showing the cellular morphology of foam samples printed at (a) 55, (b) 85, and (c) 100% flow rate.

The influence of the flow rate on the mesostructure, cellular morphology, and part density is governed by two main factors. The first one is the volumetric throughput of the expanding material from the nozzle exit relative to the amount of material needed to fully fill the space, based on the part design (raster cross-sectional size) and printing process requirements (the speed at which the raster is created, i.e., print speed). The second one is the residence time of the polymer melt inside the heater block before it exists the nozzle. In general, at a given nozzle temperature, longer residence time assures a better temperature uniformity of the melt and provides longer times for the expansion of the microspheres. Lower flow rate provides smaller volumetric throughput and longer residence time. On the other hand, higher flow rate gives sufficient or excessive throughput and shorter residence time. At the low flow rate of 55% in the case of this study, the existence of the inter-bead gaps on the surface (Figure 3a) and microstructure (Figure 4a) is attributed to the lack of sufficient material throughput. In other words, the amount of material per unit time used to form the raster is so low that even with the foam expansion, the inter-bead spaces are not fully filled, leaving the gaps behind. Also, the highest cell size at 55% flow rate is explained by the longest residence time. Therefore, the lowest flow rate provides the highest chance for the free expansion of the exiting material from the nozzle due to a longer residence time and a lower pressure between the nozzle and the underlying layer. Consequently, the lowest part density (Figure 5b) is obtained once the lowest flow rate is used. It can thus be concluded that lower flow rates are favorable in achieving foams with lower densities. However, excessively low flow rates can result in poor raster to raster bonding and substantial inter-bead gaps, which are not desired. It is

further noted that the low cell density at low flow rate case could be related to the existence of the inter-bead gaps, which contribute to the volume but not considered as cells. Another possibility for the low cell density could be the excessive residence time, probably causing the collapse of some local cells. This is due to gas loss once the microspheres are under high internal pressure for prolonged times while the system pressure (i.e., the pressure inside the heater block) is not significantly high.

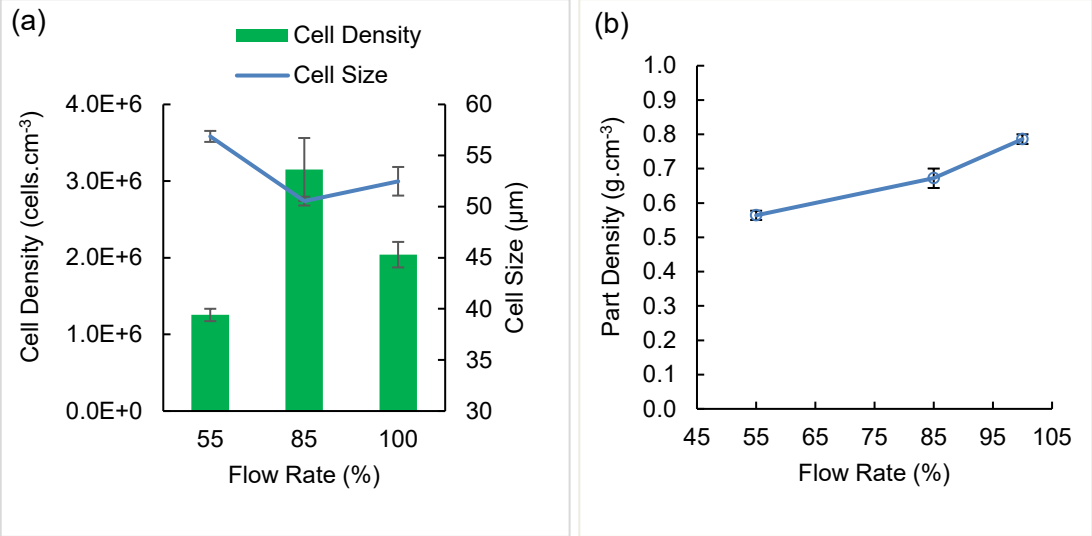

Figure 5. Effect of flow rate on (a) cell density and cell size and (b) part density. Error bars denote ±1 SD (standard deviations).

The absence of the inter-bead defects with 85% flow rate can also be explained by the above factors. 85% flow rate provides sufficient amount of material input for constructing the raster as well as sufficient amount of associated under-nozzle pressure due to the in-situ expansion of the material. These two result in completely filled raster cross-sectional geometry with good bead to bead bonding and no gaps. As the flow rate is now higher, the residence time is shorter and thus the cell sizes are smaller (Figure 5a).

The highest flow rate of 100% is obviously not a good choice for foam printing, if low densities are desired. 100% flow rate means the part should be fully made with densities close to that of solid material without any expansion. Moreover, 100% flow rate may not provide sufficient resident time for a uniform temperature distribution and TEM expansion. Therefore, a choice of 100% flow rate does not leave sufficient room for foam expansion during raster deposition. Independent of the set flow rate, the high-pressure thermally expendable microspheres expand as they exit the nozzle. This expansion coupled with the excessive amount of extruded material causes the over-extrusion of the rasters, which is clearly seen in Figure 3c as surface defects. The cell size's largest standard deviation was associated with the morphology of the 100% flow rate case (Figure 5a), indicating the nonuniformity in the cellular morphology (Figure 4c) and can be attributed to the short residence time and possible nonuniform temperature distribution and therefore nonuniform expansion. The smaller cell density values in this case may also be due to excessively short resident time such that some microspheres did not get an opportunity to expand, especially in the regions with lower temperatures. Moreover, as expected, the highest flow rate resulted in the highest density.

The effect of print speed: The second parameter studied was print speed, i.e., the velocity of the nozzle tip linear motion. Figure 6 and Figure 7 show the surface and the internal microstructure, respectively, of the foam samples, made at three print speeds. In the parts made with 5 $mm.s^{-1}$ print speed, the surface exhibited inter-bead line gaps along the print direction (Figure 6a). Similarly, anomalies in the cellular morphology are seen, as identified in Figure 7a. The increase of print speed to 25 $mm.s^{-1}$ improved both the surface and internal microstructure (Figure 6b and 7b). Further increase of print speed to 125 $mm.s^{-1}$ resulted in the formation of the huge inter-bead line gaps along the print direction (Figure 6c) and due to nonuniform expansion, the internal microstructure showed unexpanded regions, raster boundaries and nonuniform cell shapes and sizes (Figure 7c).

Figure 8a shows the cell size and cell density for the foam samples made at three print speeds. Parts printed at 5 $mm.s^{-1}$ print speed exhibited the highest cell size (54.29 µm) with the intermediate cell density (1.52×10^6 $cells.cm^{-3}$). Once the print speed was changed to 25 $mm.s^{-1}$, the average cell size dropped to 50.54 µm and the cell density was raised to 3.15×10^6 $cells.cm^{-3}$. Further increase in the print speed to 125 $mm.s^{-1}$ caused further reductions in the cell size to 45.82 µm and the cell density (0.74×10^6 $cells.cm^{-3}$). Part density with respect to the print speed is shown in Figure 8b. At 5 and 25 $mm.s^{-1}$, the part density was found to be 0.71 and 0.67 $g.cm^{-3}$, respectively, with no significant difference. However, with increase in the print speed to 125 $mm.s^{-1}$, part density was the highest, i.e. 0.95 $g.cm^{-3}$.

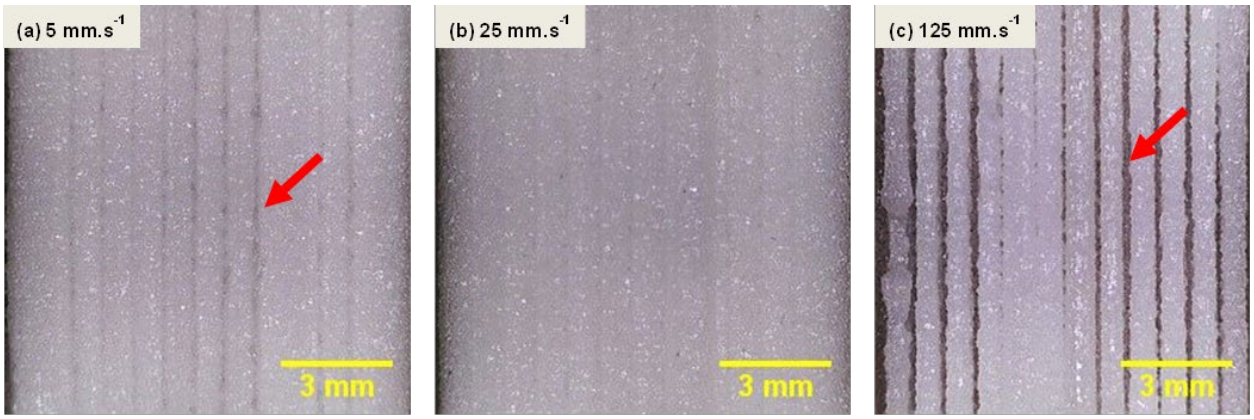

Figure 6. Optical images (Y-X plane view) showing the surface morphology of samples printed at (a) 5, (b) 25, and (c) 125 $mm.s^{-1}$ print speed.

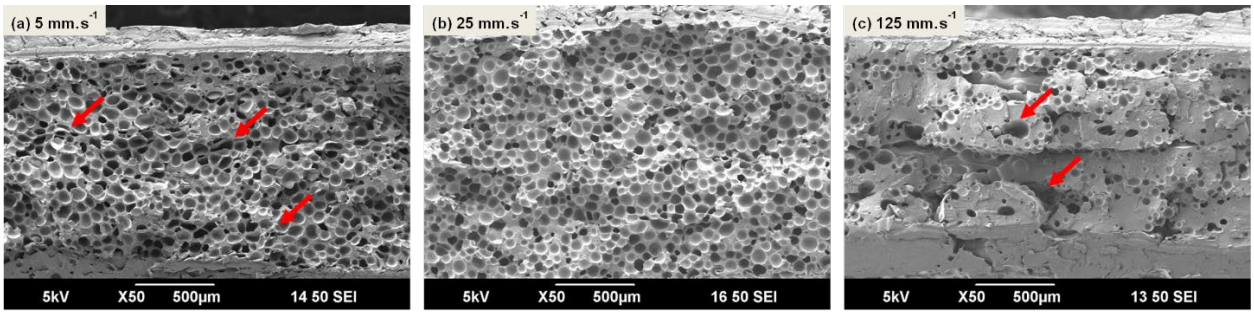

Figure 7. SEM micrographs (Y-Z plane view) showing the cellular morphology of foam samples printed at (a) 5, (b) 25, and (c) 125 $mm.s^{-1}$ print speed.

As explained previously for flow rate effect, the influence of print speed on the mesostructure, cellular morphology, and part density can also be explained by two main factors, i.e., volumetric throughput and residence time. As the print speed increases, the filament feed-in velocity increases, and thus, the melt exits nozzle at a faster rate; thereby the volumetric flow rate increases and the residence time inside the heater block decreases. At the lowest print speed, i.e., 5 $mm.s^{-1}$, the formation of inter-bead gaps on the surface (Figure 6a) and anomalies and gaps in the microstructure (Figure 7a) are likely due to excessive residence time of the microspheres and low material throughput. Very low print speed means excessive residence time that could first cause the maximum expansion of microspheres followed by their shrinkage/collapse as evident from Figure 7a (highlighted with red arrows). This resulted in the largest cell sizes together with the largest variation in the cell size. Cell density was not the highest which could be related to relatively low melt throughput and loss of some cells due to collapse.

Once the print speed was increased from 5 to 25 $mm.s^{-1}$, the cellular morphology was improved. This speed provided sufficient amount of expanded extrudate for constructing the raster as well as sufficient amount of associated bead pressures from the depositing material together with an optimum residence time. These further resulted in uniform cellular morphology and the absence of inter-bead gaps (Figure 6b and 7b). Cell density was increased indicating that a larger number of cells could be activated and preserved while the cell size slightly decreased due to overall short residence time.

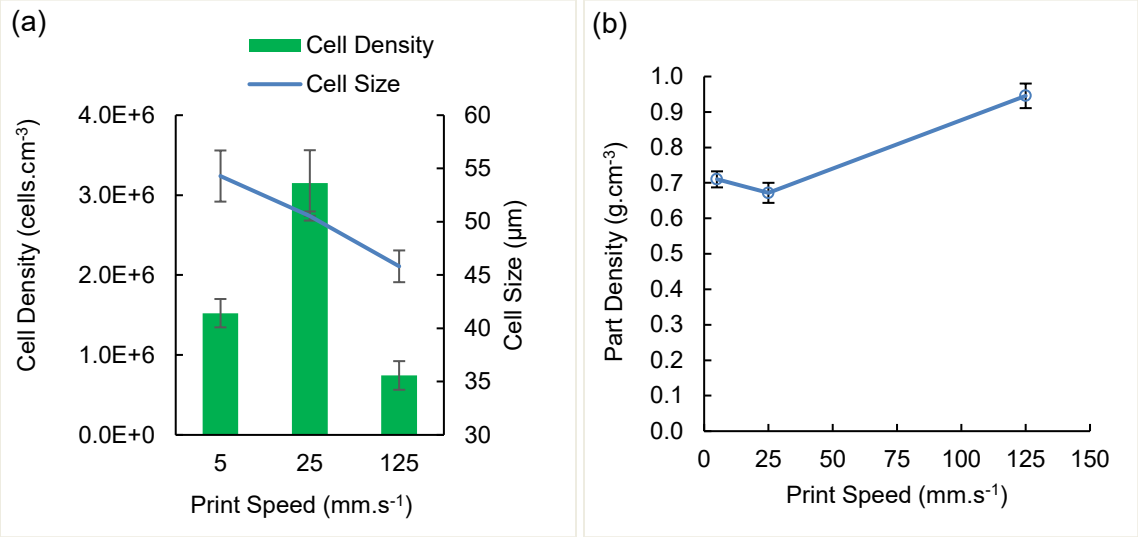

Figure 8. Effect of print speed on (a) cell density and cell size, and (b) part density. Error bars denote ±1 SD (standard deviations).

Samples printed with a speed of 125 mm.s^{-1} had significantly higher filament feed-in velocity due to which the residence time of the melt proved to be insufficient for the activation and expansion of the microspheres. Hence, this caused partial and non-uniform expansion of the depositing extrudate which resulted in the formation of huge inter-bead gaps along the print direction (Figure 6c). As shown in Figure 7c, the presence of cells with nonuniform sizes and shapes, appearance of raster boundaries with huge inter-bead gaps and unfoamed sections clearly indicate that at the high print speed of 125 mm.s^{-1}, the residence time was too short and proper foam expansion and filling could not take place. Consequently, the size and population density of the cells were found to be the lowest (Figure 8a), indicating that some microspheres did not get a chance to expand, and others expanded only partially. Due to these reasons and the presence of unfoamed sections, the part bulk density was found to be high, reaching 0.95 g.cm^{-3}. Hence, 125 mm.s^{-1} was concluded to be too high for the proper foaming, especially, if lower densities are required.

In summary, to obtain printed foams with good quality and uniform cellular morphology, the melt flow rate and the print speed should be optimized. Use of partial flow rate is an effective strategy. However, excessively low flow rate would result in the loss of structural integrity of the printed foam, due to the lack of raster to raster connections. Print speed should also not be very high as it can prevent foaming, due to insufficient residence time.

Conclusion

The purpose of this study was to investigate the effect of flow rate and print speed on the density and microcellular structure of polylactic acid (PLA) foams printed via in-situ foam fused filament fabrication (FFF) process. Unexpanded filaments loaded with thermally expandable microspheres (TEMs), at 2.5 wt.%, were prepared and FFF print process was used to print foam samples at flow rates of 55, 85 and 100% and print speeds of 5, 25 and 125 mm.s^{-1}. It was found that both flow rate and print speed have significant impact on the cellular morphology, mesostructure, surface features, and part density. At low flow rate, i.e., 55%, due to relatively longer residence time, degree of expansion was the highest which resulted in larger cell size with relatively lower part density of 0.56 g.cm^{-3}. Also, due to low throughput at this flow rate, inter-bead gaps were formed on the surface and internal microstructure. However, at higher flow rates, i.e., 85% and 100%, due to higher throughput, part densities were higher and inter-bead gaps vanished. At 100 % flow rate, part density was the highest (0.79 g.cm^{-3}) with over-extrusion and large variations in the cell size, due to the insufficient residence time. Similarly, at low print speed, i.e., 5 mm.s^{-1}, due to relatively longer residence time, anomalies in the cell shapes and sizes were observed. At the highest print speed of 125 mm.s^{-1}, due to relatively high filament feed-in velocity and short residence time, expansion of microspheres could not be fully realized and resulted in non-uniform cellular morphology as well as huge inter-bead gaps with a very high density of 0.95 g.cm^{-3}. Overall, print speed of 25 mm.s^{-1} and flow rate of 85%

proved to be optimum processing parameters to provide a relatively low density with uniform cellular morphology and no inter-bead gaps.

Acknowledgement

This material is based upon work supported by the National Science Foundation under Grant No. IIP # 1822147, Industry/University Cooperative Research Center for the Science of Heterogeneous Additive Printing of 3D Materials (I/UCRC SHAP3D). Any opinions, findings, and conclusions or recommendations expressed in this material are those of the author(s) and do not necessarily reflect the views of the National Science Foundation. The authors would also like to thank Sekisui Chemical Co. and NatureWorks LLC for providing materials.

References

[1] J. Pinto, D. Morselli, V. Bernardo, B. Notario, D. Fragouli, M.A. Rodriguez-Perez, A. Athanassiou, Nanoporous PMMA foams with templated pore size obtained by localized in situ synthesis of nanoparticles and CO2 foaming, Polymer (Guildf). 124 (2017) 176–185. https://doi.org/10.1016/j.polymer.2017.07.067.

[2] W. Zhai, J. Jiang, C.B. Park, A review on physical foaming of thermoplastic and vulcanized elastomers, Polym. Rev. (2021) 1–47. https://doi.org/10.1080/15583724.2021.1897996.

[3] T. Sadik, C. Pillon, C. Carrot, J.A. Reglero Ruiz, Dsc studies on the decomposition of chemical blowing agents based on citric acid and sodium bicarbonate, Thermochim. Acta. 659 (2018) 74–81. https://doi.org/10.1016/j.tca.2017.11.007.

[4] A. Kmetty, L. Katalin, Development of Poly (Lactide Acid) Foams with Thermally Expandable Microspheres, Polymers (Basel). (2020). https://doi.org/10.3390/polym12020463.

[5] V. Contreras, F.J. Maturana, J. Poveda, K.C. Núñez, J.C. Merino, J.M. Pastor, Optimization of injection parameters to obtain selected properties on foamed PP with hollow glass microspheres and thermally expandable microspheres using Taguchi method, J. Cell. Plast. (2020). https://doi.org/10.1177/0021955X20943097.

[6] A. Ameli, P.U. Jung, C.B. Park, Electrical properties and electromagnetic interference shielding effectiveness of polypropylene/carbon fiber composite foams, Carbon N. Y. 60 (2013) 379–391. https://doi.org/10.1016/j.carbon.2013.04.050.

[7] A. Ameli, D. Jahani, M. Nofar, P.U. Jung, C.B. Park, Development of high void fraction polylactide composite foams using injection molding: Mechanical and thermal insulation properties, Compos. Sci. Technol. 90 (2014) 88–95. https://doi.org/10.1016/j.compscitech.2013.10.019.

[8] S.T. Lee, C.B. Park, Foam Extrusion: Principles and Practice, 2nd ed., CRC Press, Taylor & Francis Group, 2014.

[9] S.T. Lee, L. Kareko, J. Jun, Study of thermoplastic PLA foam extrusion, J. Cell. Plast. 44 (2008) 293–305. https://doi.org/10.1177/0021955X08088859.

[10] B.N. Turner, S.A. Gold, A review of melt extrusion additive manufacturing processes: II. Materials, dimensional accuracy, and surface roughness, Rapid Prototyp. J. 21 (2015) 250–261. https://doi.org/10.1108/RPJ-02-2013-0017.

[11] M. Nofar, J. Utz, N. Geis, V. Altstädt, H. Ruckdäschel, Foam 3D Printing of Thermoplastics : A Symbiosis of Additive Manufacturing and Foaming Technology, 2105701 (2022) 1–18. https://doi.org/10.1002/advs.202105701.

[12] Y. Li, Z. Feng, L. Hao, L. Huang, C. Xin, Y. Wang, E. Bilotti, K. Essa, H. Zhang, Z. Li, F. Yan, T. Peijs, A Review on Functionally Graded Materials and Structures via Additive Manufacturing: From Multi-Scale Design to Versatile Functional Properties, Adv. Mater. Technol. 5 (2020). https://doi.org/10.1002/admt.201900981.

[13] B.K. Park, C.-J. Kim, D.E. Kwon, Y.-W. Lee, Design and Fabrication of Partially Foamed Grid Structure Using Additive Manufacturing and Solid State Foaming, Processes. (2020). https://doi.org/10.3390/pr8121594.

[14] J. Wang, H. Xie, Z. Weng, T. Senthil, L. Wu, A novel approach to improve mechanical properties of parts fabricated by fused deposition modeling, Mater. Des. 105 (2016) 152–159. https://doi.org/10.1016/j.matdes.2016.05.078.

[15] M. Li, J. Jiang, B. Hu, W. Zhai, Fused deposition modeling of hierarchical porous polyetherimide assisted by an in-situ CO2 foaming technology, Compos. Sci. Technol. 200 (2020) 108454.

https://doi.org/10.1016/j.compscitech.2020.108454.
[16] A.R. Damanpack, A. Sousa, M. Bodaghi, Porous PLAs with Controllable Density by FDM 3D Printing and Chemical Foaming Agent, Micromachines. 12 (2021) 866. https://doi.org/10.3390/mi12080866.
[17] H. Andersson, J. Ortegren, R. Zhang, M. Grauers, H. Olin, Variable low-density polylactic acid and microsphere composite material for additive manufacturing, Addit. Manuf. 40 (2021). https://doi.org/10.1016/j.addma.2021.101925.
[18] K. Kalia, B. Francoeur, A. Amirkhizi, A. Ameli, In Situ Foam 3D Printing of Microcellular Structures Using Material Extrusion Additive Manufacturing, ACS Appl. Mater. Interfaces. 14 (2022) 22454–22465. https://doi.org/10.1021/acsami.2c03014.
[19] P.K. Penumakala, J. Santo, A. Thomas, A critical review on the fused deposition modeling of thermoplastic polymer composites, Compos. Part B. (2020). https://doi.org/10.1016/j.compositesb.2020.108336.
[20] K. Kalia, A. Ameli, Effect of carbon fiber on the fracture toughness of fused filament fabricated CF/ABS composites, in: ANTEC 2021 (Ed.), Annu. Tech. Conf. - ANTEC, Conf. Proc. (Vol. 2021-May). Soc. Plast. Eng., 2021.
[21] H.S. Podyman, Y.H. Dvoinos, V.A. Novik, Modeling the homogenization process of polyethylene compositions in a single-screw extruder with a Maddock mixing element, in: Mech. Compos. Mater., 2021: pp. 517–526. https://doi.org/10.1007/s11029-021-09974-x.